Adapting a Foggy Future along Trans-Arctic Shipping Routes

Shutong song
https://orcid.org/0000-0003-3718-001X
Yue Chen
Ocean University of China
Xianyao Chen (chenxy@ouc.edu.cn)
Ocean University of China https://orcid.org/0000-0001-9825-5295
Changshuo Chen
Geovis Technology Company Limited
King-Fai Li
UC Riverside https://orcid.org/0000-0003-0150-2910
Ka-Kit Tung
University of Washington https://orcid.org/0000-0001-8667-7167
Qiuli Shao
nstitute of Oceanographic Instrumentation, Qilu University of Technology (Shandong Academy of Sciences)
Yilin Liu
Ocean University of china
Xiaoyu Wang
Ocean University of china
Li Yi
Ocean University of china
Jinping Zhao
Ocean University of China

Article

Keywords:

Posted Date: February 9th, 2022

DOI: https://doi.org/10.21203/rs.3.rs-1313169/v1

Adapting a Foggy Future along Trans-Arctic Shipping Routes

Shutong Song[1,2], Yue Chen[1,2], Xianyao Chen[1,2,*], Changshuo Chen[3], King-Fai Li[4], Ka-Kit Tung[5], Qiuli Shao[2], Yilin Liu[1], Xiaoyu Wang[1], Li Yi[1], Jinping Zhao[1,2]

[1] Frontiers Science Center for Deep Ocean Multispheres and Earth System, Key Laboratory of Physical Oceanography, College of Oceanic and Atmospheric Sciences, Ocean University of China, Qingdao, China

[2] Qingdao National Laboratory for Marine Science and Technology, Qingdao, China.

[3] Geovis Technology Company Limited, Beijing, China

[4] Department of Environmental Sciences, University of California, Riverside, Riverside, California, US

[5] Department of Applied Mathematics, University of Washington, Seattle, Washington, US

*Corresponding author: Xianyao Chen (chenxy@ouc.edu.cn)

Abstract

Rapid retreat of Arctic sea ice extent in response to global climate warming expends the area of open ocean for new trans-Arctic shipping routes. Ship companies will benefit from the shortened sailing distance across the Arctic, but threats of intensified sea fog induced by the retreated sea ice, especially the potential risk of accidents due to low visibility, are not well considered when designing the trans-Arctic shipping routes. Here, we show that the sailing time along the previous suggested routes will increase nearly 10–30% caused by the impacts of sea fog. We further design a new route detouring to the low-fog-frequency area, based on the projected sea ice extent and the fog frequency in 21st century. The new route is 5–20% longer than the original one, but can save as much as 10% of total sailing time, and most importantly, will lower the risk of catastrophic accidents. Our estimates are similar in both RCP4.5 and 8.5 of CMIP5 simulations.

Impacts of fog on Arctic shipping routes

The increase of open water area as a result of the sea ice retreat has inadvertently attracted socio-economic developments in the Arctic, such as oil extraction, North Pole tourism, and trans-Arctic shipping routes[1–4]. The latter have particularly received international interests after the 2021 Suez Canal Blockage. Ship companies can realize the greatest advantage, because present travels of more than 20,000 km from Far East to Northwest Europe via the Suez Canal can be reduced to about 10,000 km and the averaged sailing times can be shortened from 20 days to 11 days, if the Northern Sea Route (NSR) north of the Russian Federation through the Arctic is used[4-6]. It is estimated that by the mid-21th century, changing sea ice conditions will enable expanded September navigability for common open-water vessels crossing the Arctic along the NSR, as well as robust new routes for moderately ice-strengthened (Polar Class 6, PC6) vessels over the North Pole, and new routes through the Northwest Passage (NWP) for both classes[6–10]. Taking into account canal fees, fuel costs, and other variables that determine freight rates, this shortcut can tremendously reduce the costs of a large container ship company every year. The savings would be even higher for megaships that are unable to pass through Panama and Suez Canals and so currently still sail around the Cape of Good Hope and Cape Horn[11].

However, the occurrence of fog may slow down or even stop these marine operations, leading to significant economic costs[12]. Although vessels equipped with cutting-edge instruments such as radar, searchlights, and radios can avoid collisions if they exactly follow International Maritime Organization regulations during transportation, low visibility under the sea fog may increase the chances of judgment errors and threaten the operation of common open-water vessels and even the vessels of PC6 while navigating in the ocean with floating ice. Previous assessments of future optimal navigation routes in Arctic are mostly based on the sea ice conditions under the representative concentration pathway (RCP) 4.5 and 8.5 climate-forcing scenarios[10,13]. The impact of sea fog on navigation routes are not considered. Here, we use a combination of present-day reanalysis and model simulations to project sea fog

variability in 21st century and design new routes based on the sea ice extent and sea fog changes.

Projected Arctic sea fog

Direct simulation of sea fog using Polar-optimized version of the Weather Research and Forecasting Model (PWRF) requires 6-hourly atmospheric fields, with a 25-hPa vertical resolution within the boundary layer, as the initial and boundary conditions. This kind of data is usually unavailable in future projections based on the Fifth Phase of the Coupled Model Intercomparison Project (CMIP5). To project the future Arctic sea fog variability, we first simulate the present-day Arctic sea fog frequency (SFF) using PWRF with 6-hourly atmospheric fields from ERA-Interim reanalysis datasets[14] (PWRF-ERA). Then, based on this present-day simulation, we derive a semi-empirical multi-variable linear relationship between the Arctic SFF with the relative humidity (RH) and atmospheric stability, defined as the temperature inversion between 925 hPa and 2 m above ground (Methods). Finally, the future Arctic SFF is estimated using the CMIP5 RH and atmospheric stability and the derived semi-empirical multilinear relationships.

We define SFF as the fraction of Arctic sea fog days in each summer (July to September)[15,16]. A day is defined as fog day, if at least one 6-hourly model output in this day is foggy. Based on the simulations of PWRF-ERA, the SFF is highly correlated ($\geqslant$ 0.7) with the summer-mean RH over most of the Arctic Ocean except the north Beaufort Sea (Figure S1). The strong correlation between SFF and RH is expected because high RH, which means that atmosphere approaches 100% more frequently (Figure S2), is a necessary but not sufficient condition for onset of fog[17]. Atmospheric stability is another necessary condition for onset of fog over the north Beaufort Sea, where the atmospheric stability is shown to be well correlated with SFF (~0.4; Figure S1). The simulation suggests that a northward-propagating Beaufort high-pressure center enhances local atmospheric stability while an eastward-propagating Beaufort high enhances the local RH (Figure S3). The spatial pattern of future SFF during 2006–2099 is derived from the monthly mean of 21

89 climate models in CMIP5 under RCP 4.5 and 8.5. The ensemble mean of projected
90 SFF in 21st century exhibits similar pattern with nowadays ship-based observations[18]
91 and previous studies[19,20]: SFF along the coast is higher than 20%, especially over
92 north of Alaska, Canadian Arctic Archipelago, Greenland Sea, and East Siberian Sea.
93 In the central Arctic, it decreases rapidly and is only about 6% near North Pole
94 (Figure 1a-d). The high SFF along the coast and over central Arctic is related to the
95 great temperature gradient between warm land and cool sea surface along the coast
96 during summer, which enhances advection fog formation when warm and moist air
97 cools and condensates over cold water[21–23]. Compared with observations, the
98 simulated fog captures the spatial characteristics on the Atlantic side, but it is about 10%
99 larger than observation along Alaska coast and Canadian Arctic Archipelago. This
100 over-estimation is mainly because the liquid water content in the model simulation is
101 always greater than the observations[24].
102 Historical SFF over entire Arctic Ocean north of 70ºN during the past 40 years
103 simulated by PWRF-ERA exhibits significant linear decreasing trend by –0.4% every
104 decade (Figure 1e). While more open water due to surface warming increases
105 evaporation and specific humidity in the air, the increased partial pressure of water
106 vapor does not necessary infer increased fog formation because the saturation vapor
107 pressure also increases in the warming air. In fact, fog formation may even decrease if
108 the saturation vapor pressure increases faster than the partial pressure of water vapor,
109 especially over the open water area (Figure 1f). As a result, different climate models
110 may predict widely different future sea fog variability. GFDL-CM3 shows that SFF
111 remains nearly unchanged in 21st century, whereas in CNRM-CM5 it is reduced by
112 about one third during this century. The ensemble-mean of model SFF significantly
113 decreases by –0.2% every decade, similar to the decreasing trend during past 40 years.
114 While the averaged SFF over the entire Arctic may decrease as a result of the
115 Arctic warming and the Clausius–Clapeyron relation, the PWRF-ERA simulation
116 suggests that SFF increases more than 10% over the new open water regions (Figure
117 1g), mostly because of an increase of moisture and latent heat exchange between the

Arctic air and the relatively warm Arctic sea surface[25]. We also find that the SFF usually increases substantially over the new open water regions where the SIE is more than 40% in previous year (Figure 1g), or some regions where the sea ice melts rapidly but still exists (Figure S4). It should be noted that these new open water regions are generally chosen as the new routes[10] because ships tend to pass through the area with sea-ice melting in higher latitude to save distance. Therefore, the impact of sea fog to the Arctic routes must be considered.

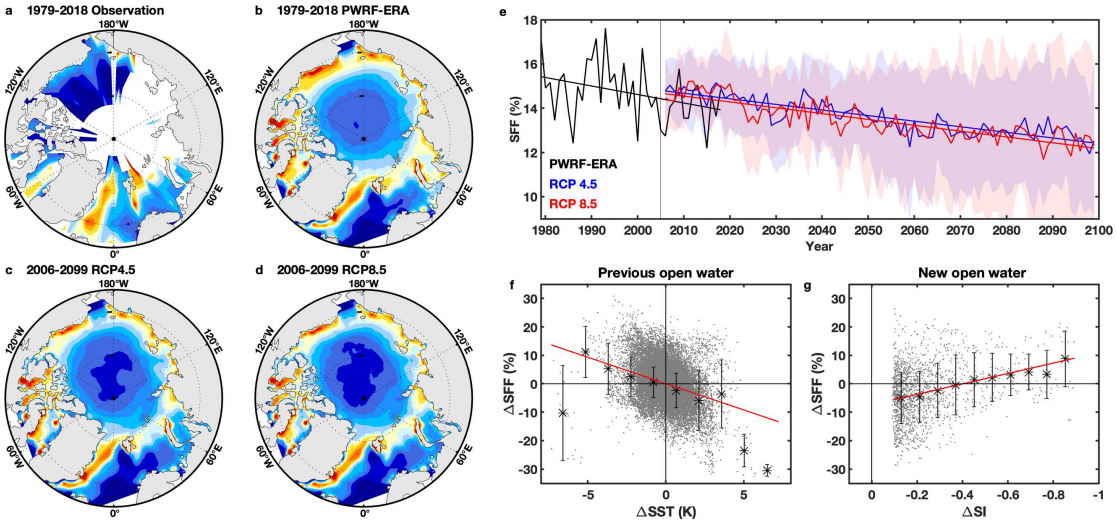

Figure 1. Climatological distribution and variability of Arctic summer SFF. (a) and (b) are results from ship observation and PWRF-ERA. The shaded grid in (a) represents observation with data more than 10 years. (c), (d) are the projected SFF under RCP4.5 and 8.5 during 2006-2099. (e) shows the regional-averaged SFF over the sea north of 7º0N based on PWRF-ERA (black), RCP4.5 (blue) and 8.5 (red). Shading indicates ±one standard deviation. The linear trends pass the Mann-Kendall test under 95% significance level. (f) shows the fog change and SST change over regions which are open water in previous and current years. (g) shows the relationship between fog and sea ice change over regions where sea ice in previous year is larger than 10% and will melt into open water in current year (sea ice less than 1%). Error bars denote one standard deviation. (f) and (g) are based on PWRF-ERA.

Previous studies have designed many trans-Arctic routes for polar-class and open-water vessels with medium and no ice-breaking capability based on sea ice conditions only[7,10,13,26]. The potential routes, including the NSR along the north of the Russian Federation and the NWP via the Canadian Arctic Archipelago, will be navigable owing to the rapid retreat of sea ice. In order to estimate the impacts of sea fog on transit time along these routes, we first employ the same method to derive the trans-Arctic routes for a moderately ice-strengthened ship (Table S3) in nine non-overlapping 10-year segments from 2006 to 2095, using CMIP5 multi-model ensemble mean of sea ice under RCP4.5 and 8.5 (hereafter referred as Route-I).

Consistent with the previous plans[7,10], Route-I, starting from Rotterdam or St. John's and terminating at Bering Strait, tends to shift to higher latitudes and will go through central Arctic Ocean by midcentury under the Arctic warming (Figure 3 and S6). Due to the shorter sailing distance, the sailing time of Route-I decreases from 12 days during 2006-2015 to 10 days during 2086-2095 along the NSR, and decreases from 12 days to 11 days along the NWP (Figure 2). The total distance travelled in the proposed NSR and NWP routes terminating at Bering Strait shown in Figure 3 are generally of the order of 4000 km.

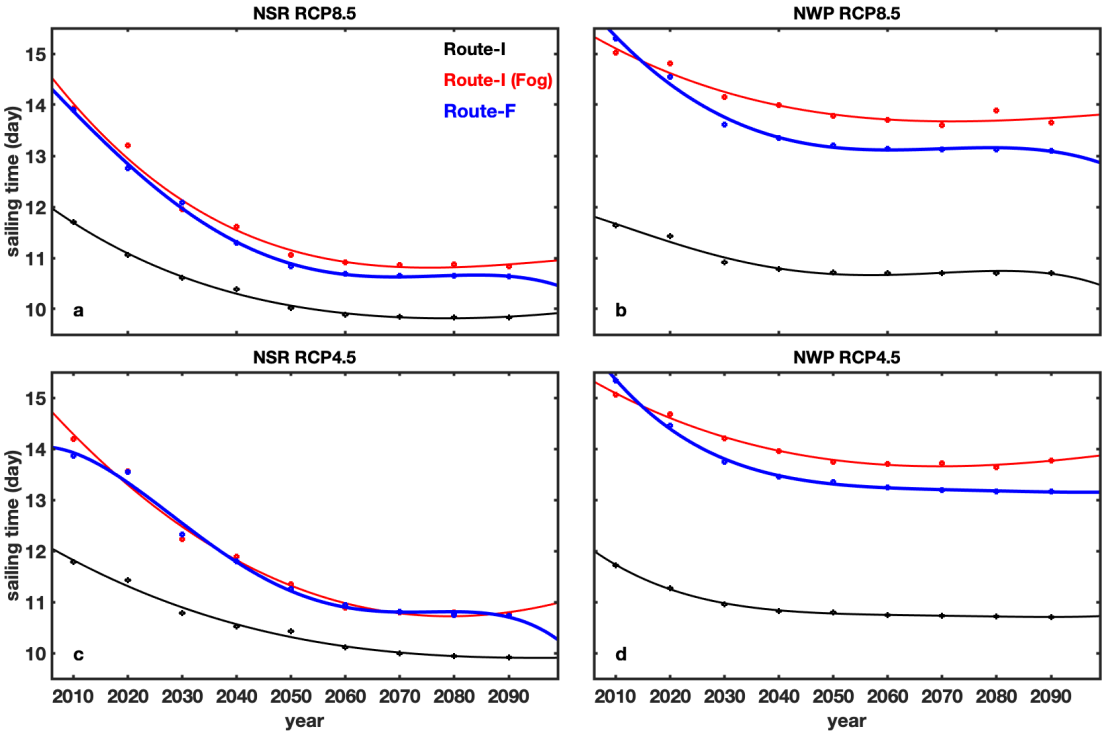

Figure 2. Sailing time along Northern Sea Route (NSR) and North West Passage (NWP) under RCP4.5 and 8.5. Solid blue lines indicate Route-I that only considering sea ice; Dashed blue lines indicate Route-I but considering the deceleration of sea fog. Red lines indicate Route-F considering both sea ice and sea fog. The sailing time at 2010 represents the mean result during 2006-2015, and so on.

To show the SFF along the proposed routes, we use the cumulative distance travelled from Rotterdam or St. John's as the abscissa along the routes. Both NSR and NWP experience frequent sea fog. During 2006–2015, there are more than 740 km of the voyage along NSR with SFF exceeding 20% (defined as high-SFF region). These regions are mainly located in the Barents Sea (1500-2000 km from the starting city) and the East Siberian Sea (3200-3700 km). Along the routes, the maximum SFF can reach 23.0% and 24.1%, respectively (Figure 4a), posing higher risk on the ship operations. With sea ice melting, NSR shifts to higher latitude, and sea fog along NSR may decrease when the saturation vapor pressure increases in the warming air. The high-SFF region during 2086-2095 becomes about 520 km, reduced by 30% compared with that during the early century. However, the maximum SFF can still reach more than 30%, mainly in Frame Strait (1500-2000 km), which cannot be ignored by shipping planning.

The high-SFF regions along NWP can reach about 1330 km, more than double than that along NSR (Figure 4b). Most of them are located in Baffin Bay (1600–2000 km) and north of Alaska (3000–3800 km). The maximum SFF in these two regions are 34.1% and 34.6%, respectively. The SFF distribution along NWP is almost unchanged in 21st century while the pathway of NWP and the SFF along NWP are basically unchanged.

Obviously, both NSR and NWP are inevitably affected by sea fog in the current century. The sea fog along NWP is particularly frequent and persistent. A northward shift of the NSR may avoid some of the fog along the route, but some high-SFF regions are still included in the potential routes. For this reason, even

though the previous proposed NWP and NSR are the shortest paths given the projected sea ice extent, the sailing time of Route-I will actually be much longer if taking the frequent sea fog into account.

To quantify the effect of sea fog on Route-I, we assume that the ship will slow down when running into the sea fog and introduce a deceleration coefficient to demonstrate that the higher fog frequency at a given location, the greater the deceleration of ships will be (Table S5). Using the deceleration coefficient, we estimate that along the NSR, the total sailing time will increase by 10–20% if using the previous planned routes (Figure 2). In 2020s, the impact of sea fog may reduce the shipping speed and spend more than 2 days than previous estimations. The sea fog tends to decrease because atmosphere is difficult to saturate in the warmer Arctic in the future, but the sailing time can still increase about 1 day after 2050s. Along the NWP, the impact of sea fog is more serious, the total sailing time is about 2.5–3.5 days (25–30%) longer than the previous estimation during this century. These estimations are similar between RCP4.5 and 8.5.

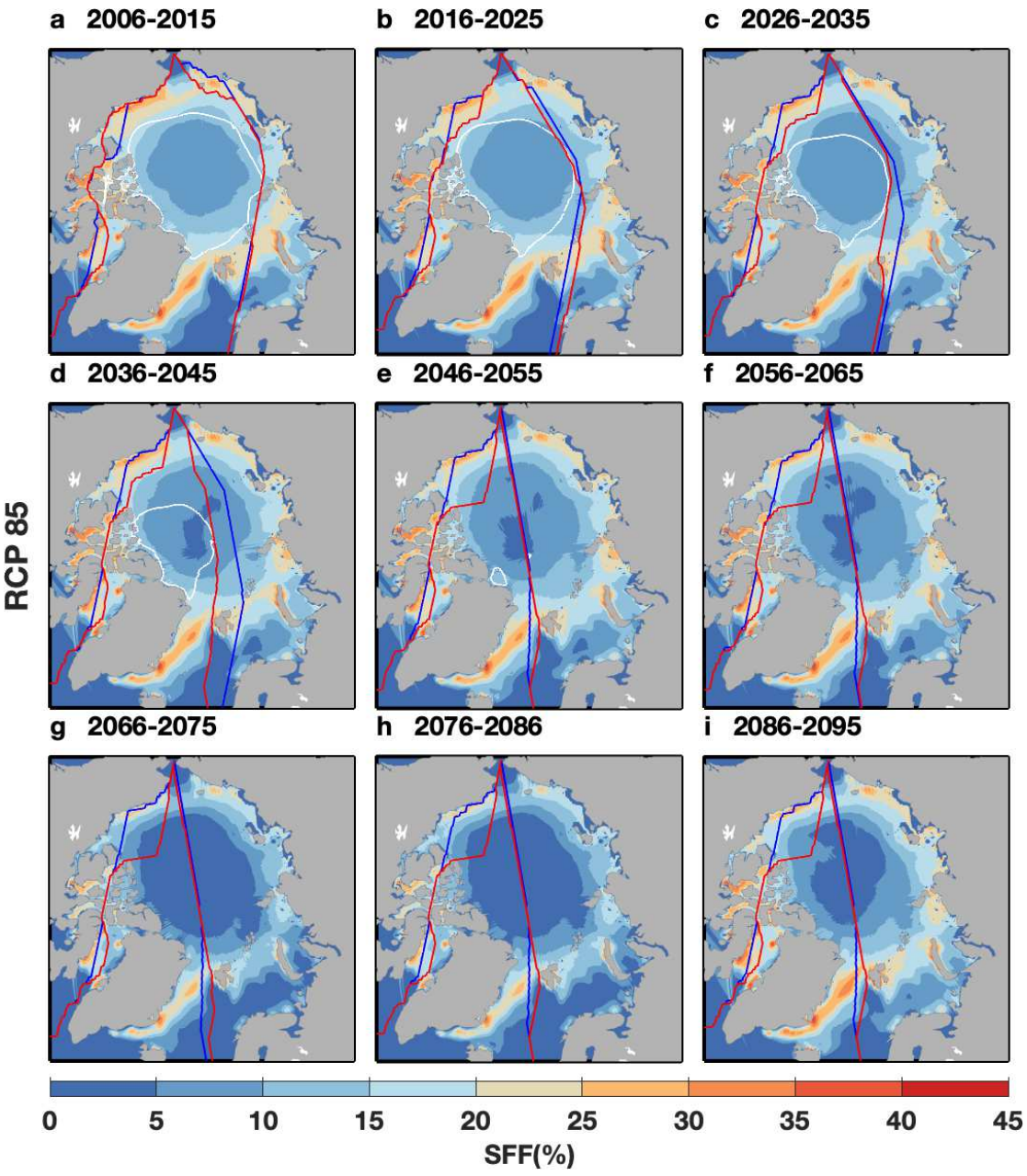

Figure 3. The comparison between the Route-I and the Route-F along NSR and NWP every decade under RCP8.5. Blue line represents Route-I, while the red one Route-F. White line indicates is the isopleth of 45% sea ice concentration. Color bar indicates the spatial distribution of projected SFF.

208 **Shipping routes with impacts of sea fog**

209 In order to reduce the impacts of sea fog, Route-I must be re-optimized given
210 the constraint of the projected sea fog. We develop a new cost function based on the
211 different speed of ships inside and outside of the sea fog area, and the different sea ice
212 condition, to design a new trans-Arctic route. The new route with shortest time is
213 derived and referred as Route-F (See Methods and Figure S6). Based on the CMIP5
214 multi-model ensemble means of sea ice and SFF, we compute the path and sailing
215 time of Route-F every ten years.

216 Along the NSR, the sailing time of Route-F only shortens by 0.2 day on
217 average compared with the Route-I in 21st century under RCP8.5 (Figure 2). The
218 shortening is due to different factors before and after midcentury. During the period
219 from 2036 to 2045, Route-F tends to avoid high-SFF region along the Eurasian coast
220 to navigate at higher latitudes under RCP8.5 (Figure 3). The northward shift of
221 Route-F decreases the mean fog frequency along the whole route by 1.7%, which is
222 equivalent to reducing the sailing distance by 70 km and saves sailing time by 0.3 day.
223 In contrast, after the midcentury, although both Route-F and Route-I go through the
224 ice-free central Arctic Ocean, Route-F tends to avoid the high-SFF region along the
225 northeast coast of Greenland and shifts eastward to the Fram Strait. As an example,
226 the shift of Route-F during 2086–2095 decreases the maximum fog frequency over
227 1500–2000 km segment from 29% to 22% (Figure 4c) and saves sailing time by 0.2
228 day. Compared with RCP8.5, the shift of Route-F is similar (Figure S7,8) but little
229 time saved is under RCP4.5 (Figure 2c).

230 Along the NWP, the sailing time of Route-F shortens by 0.5–1 day compared
231 with the Route-I in 21st century under both RCP (Figure 2). Constrained by the
232 locations of the islands, the path of Route-F remains nearly unchanged, except the
233 northward shift at Baffin Bay and Alaska coast to avoid high-SFF regions (Figure 3).
234 The shift at Baffin Bay segment (1600–2000 km) is within the stable range in the
235 whole century and reduces mean SFF over this segment by 4%. On the contrary, the
236 shift along Alaska coast segment (3000–3800 km) becomes more and more obvious

due to the retreat of sea ice over Beaufort Sea. By the end of century, mean fog frequency over this segment will decrease by 13% (Figure 4d). Although the length of Route-F is about 117 km longer than Route-I, it still saves sailing time up to 1 day for the lack of sea fog. This feature is also similar in RCP4.5 (Figure S8).

We further compare the Route-F with the traditional routes such as Suez Canal and Panama Canal (Table S6). These routes start from Shanghai and terminate at St. John's and Rotterdam. The result shows that Route-F saves more than 30% of distance and 20% of time of traditional routes on average in 21st century, suggesting great economic benefits of Route-F.

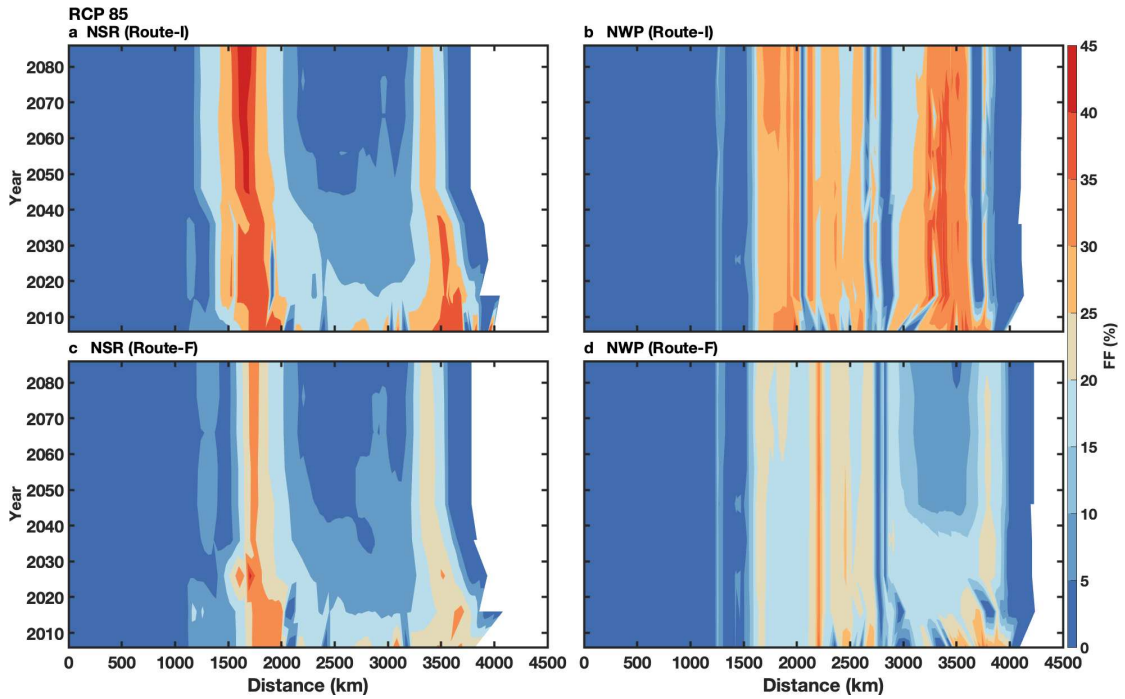

Figure 4. The variation of SFF over Route-I and the Route-F along NSR and NWP under RCP8.5. Rotterdam is the origin of NSR and St. John's the origin of NWP. Terminal is Bering Strait.

Conclusions

In summary, we found that the sailing time of Route-I will be extended by 10-30% if the impacts of sea fog are involved. But it can be improved by designing the new route (Route-F) with lower-SFF region, which can save about 0.2-1 days.

This result highlights the importance of the Arctic sea fog when designing the trans-Arctic shipping lanes in future when the Arctic sea ice continuous declining but still covers NSR and NWP to some extents.

Our analysis only considers the situation that ships pass Arctic Ocean directly without calling port. In fact, if sea fog occurs when a ship calls at a port, the ship will not only be unable to travel, but also need to pay high parking fee in ports. Therefore, our estimation is actually the minimum saving when designing trans-Arctic routes for commercial shipping companies.

References

1. Comiso, J. C., Parkinson, C. L., Gersten, R. & Stock, L. Accelerated decline in the Arctic sea ice cover. *Geophys. Res. Lett.* **35**, 1–6 (2008).
2. Barnhart, K. R., Miller, C. R., Overeem, I. & Kay, J. E. Mapping the future expansion of Arctic open water. *Nat. Clim. Chang.* **6**, 280–285 (2016).
3. Stroeve, J., Holland, M. M., Meier, W., Scambos, T. & Serreze, M. Arctic sea ice decline: Faster than forecast. *Geophys. Res. Lett.* **34**, 1–5 (2007).
4. Council, A. *et al. Arctic Marine Shipping Assessment 2009 Report*. (2009).
5. Schøyen, H. & Bråthen, S. The Northern Sea Route versus the Suez Canal: cases from bulk shipping. *J. Transp. Geogr.* **19**, 977–983 (2011).
6. Aksenov, Y. *et al.* On the future navigability of Arctic sea routes: High-resolution projections of the Arctic Ocean and sea ice. *Mar. Policy* **75**, 300–317 (2017).
7. Melia, N., Haines, K. & Hawkins, E. Sea ice decline and 21st century trans-Arctic shipping routes. *Geophys. Res. Lett.* **43**, 9720–9728 (2016).
8. Wei, T., Yan, Q., Qi, W., Ding, M. & Wang, C. Projections of Arctic sea ice conditions and shipping routes in the twenty-first century using CMIP6 forcing scenarios. *Environ. Res. Lett.* (2020) doi:10.1088/1748-9326/abb2c8.
9. Stephenson, S. R. & Pincus, R. Challenges of Sea-Ice Prediction for Arctic Marine Policy and Planning. *J. Borderl. Stud.* **33**, 255–272 (2018).

10. Smith, L. C. & Stephenson, S. R. New Trans-Arctic shipping routes navigable by midcentury. *Proc. Natl. Acad. Sci. U. S. A.* **110**, 6–10 (2013).
11. Hong, N. The melting Arctic and its impact on China's maritime transport. *Res. Transp. Econ.* **35**, (2012).
12. Buixadé Farré, A. *et al.* Commercial Arctic shipping through the Northeast Passage: routes, resources, governance, technology, and infrastructure. *Polar Geogr.* **37**, 298–324 (2014).
13. Li, Z., Ringsberg, J. W. & Rita, F. A voyage planning tool for ships sailing between Europe and Asia via the Arctic. *Ships Offshore Struct.* **15**, S10–S19 (2021).
14. Dee, D. P. *et al.* The ERA-Interim reanalysis : configuration and performance of the data assimilation system. *Q. J. R. Meteorol. Soc* 553–597 (2011) doi:10.1002/qj.828.
15. Hanesiak, J. M. & Wang, X. L. Adverse-weather trends in the Canadian Arctic. *J. Clim.* **18**, 3140–3156 (2005).
16. Sugimoto, S., Sato, T. & Nakamura, K. Effects of synoptic-scale control on long-term declining trends of summer fog frequency over the pacific side of Hokkaido Island. *J. Appl. Meteorol. Climatol.* **52**, 2226–2242 (2013).
17. Isaac, G. A., Bullock, T., Beale, J. & Beale, S. Characterizing and predicting marine fog offshore newfoundland and labrador. *Weather Forecast.* **35**, 347–365 (2020).
18. Freeman, E. *et al.* ICOADS Release 3.0: a major update to the historical marine climate record. *Int. J. Climatol.* **37**, 2211–2232 (2017).
19. Eastman, R. & Warren, S. G. Interannual Variations of Arctic Cloud Types in Relation to Sea Ice. *J. Clim.* **23**, 4216–4232 (2010).
20. Koračin, D. & Dorman, C. E. *Marine Fog: Challenges and Advancements in Observations, Modeling, and Forecasting*. (Springer International Publishing, 2017). doi:10.1007/978-3-319-45229-6.
21. Gilson, G. F., Jiskoot, H., Cassano, J. J., Gultepe, I. & James, T. D. The

Thermodynamic Structure of Arctic Coastal Fog Occurring During the Melt Season over East Greenland. *Boundary-Layer Meteorol.* **168**, 443–467 (2018).

22. Herman, G. & Goody, R. Formation and Persistence of Summertime Arctic Stratus Clouds. *J. Atmos. Sci.* **33**, 1537–1553 (1976).

23. Curry, J. A., Rossow, W. B., Randall, D. & Schramm, J. L. Overview of arctic cloud and radiation characteristics. *Journal of Climate* vol. 9 1731–1764 (1996).

24. Chen, C. *et al.* Boundary Layer Parameterizations to Simulate Fog Over Atlantic Canada Waters. *Earth Sp. Sci.* **7**, (2020).

25. Bintanja, R. & Selten, F. M. Future increases in Arctic precipitation linked to local evaporation and sea-ice retreat. *Nature* **509**, 479–482 (2014).

26. Nam, J. H. *et al.* Simulation of optimal arctic routes using a numerical sea ice model based on an ice-coupled ocean circulation method. *Int. J. Nav. Archit. Ocean Eng.* **5**, 210–226 (2013).

Methods

Data

We use observational data from International Comprehensive Ocean-Atmosphere Data Set (ICOADS)[18] to compute Arctic SFF during 1979-2018.

We use the 6-hourly daily European Centre for Medium-Range Weather Forecasts (ERA Interim)[14] during 1979-2018 as initial and boundary conditions to run regional climate model.

For projection of sea fog change in future, we use monthly sea ice concertation, sea ice thickness, RH and atmospheric stability from 21 climate models in CMIP5 during 2006-2099 under RCP4.5 and 8.5. Climate models include ACCSESS1.0, ACCSESS1.3, HADGEM-CC, HADGEM-ES, CCSM4, GFDL-CM3, MPI-ESM-MR, MPI-ESM-LR, IPSL-CM5A-MR, IPSL-CM5A-LR, MIROC5, MIROC-ESM, MIROC-ESM-CHEN, FGOALS-S2, CanESM2, GISS-E2-H, GISS-E2-H-CC, GISS-E2-R, GISS-E2-R-CC, CNRM-CM5 and MRI-CGCM3.

Model simulation of sea fog in PWRF-ERA

The state-of-the-art high resolution regional scale atmospheric model, polar-optimized version of the Weather Research and Forecasting Model (PWRF) is applied to simulate Arctic weather change[27]. Here, we simulate sea fog over Arctic during 1979-2018 using PWRF with initial and boundary conditions from ERA-interim (PWRF-ERA). Model settings and physics options[28–31] (Table S1) are same as previous study about simulating Arctic cloud[32]. To arrive at a binary fog result from the model output, five diagnostic schemes are used, including SW99[33], FSL[34], UPP (NCEP's Unified Post Processor version 2.2), G2006[35] and G2009[36] (Table S2). The fog frequency is calculated as the average of the five diagnostic schemes.

The raw fog frequency simulated by PWRF-ERA has similar spatial distribution with observations, but its magnitude is about twice as large as the observations (Figure S1). Here we used the quantile mapping (QM) bias adjustment method to adjust this model bias, which has been widely used in bias correction of

regional climate models[37]. The QM adjusts for errors in the shape of distribution of the modeled data with reference to the observed distribution. For a value in the modeled data, its quantile with respect to the distribution is estimated. Then we can find a value in observation data correspond to the similar quantile. A ratio of observation to model value is calculated to be used for the modeled value adjustment as follows

$$R = \frac{SFF_{obs}(q)}{SFF_{sim}(q)} \quad (1)$$

$$SFF_{corr}(q) = R \cdot F_{sim}(q) \quad (2)$$

where *SFF* is the fog frequency, q is the q^{th} quantile, the factor R is applied to adjust the raw modeled values of the similar quantile outside the reference period. The adjusted SFF of PWRF-ERA is used in the paper.

Projecting sea fog in CMIP5

Based on results of PWRF-ERA, the monthly SFF can be projected upon monthly RH and atmospheric stability (defined as the temperature difference between 925 hPa and 2 m) using least squares linear regression method over the year 1979-2018. SFF for each position *x*, each year *t* and each model *m* can be written as

$$SFF(x, t, m) = k_1(x) * RH(x, t, m) + k_2(x) * stability(x, t, m) + b(x) \quad (3)$$

The spatial patterns $k_1(x)$ and $k_2(x)$ are shown in Figure S4. With these linear regression coefficients, we project the future SFF(*x*, *t, m*) using the monthly mean RH(*x*, *t, m*) and stability(*x*, *t, m*) in CMIP5 during 2006-2099. To remove the difference of reference RH among climate models and reanalysis data, we make sure that the mean RH(*x, m*) during 2006-2018 in each model is consistent with mean RH(*x*) during 2006-2018 in PWRF-ERA. The same method is also used to deal with atmospheric stability.

Deriving shipping routes

Our study focuses on the peak navigation months from July to September, when vessels in Arctic reach their maximum accessibility. The 21 multi-model

average sea ice concentration and thickness are taken as the initial sea ice field. Since the spatial resolution of sea ice condition differs in different model in CMIP5, we interpolate it to a resolution of 0.5º longitude by 0.5º latitude, which can reflect the sea ice condition in the Canadian Arctic Archipelago in detail. A vessel class of PC6 is chosen for route calculation (Table S3), which is equivalent to "Type A" in Table S4. PC6-class vessel can operate in summer and autumn, crossing medium first-year ice which may include old ice inclusions[38].

A ship-routing algorithm is based on the Arctic Ice Shipping System[38]. The flowchart of the algorithm is given in Figure S6. The parameter Ice Numeral (IN) is defined to assess navigation safety in ice-covered waters[38], which is computed as follows

$$\mathrm{IN} = (\mathrm{C_a} * \mathrm{IM_a}) + (\mathrm{C_b} * \mathrm{IM_b}) + \cdots + (\mathrm{C_n} * \mathrm{IM_n}) \quad (4)$$

where $\mathrm{C_a}$ and $\mathrm{IM_a}$ are the tenths of concentration and ice Multiplier for ice type (Table S4). If the IN is negative, the vessel should not proceed and need to take an alternate route.

In the navigable area with fragmented ice, we introduce the ice resistance model proposed by Colbourne[39] to slow down the shipping speed in ice area. Here, we introduce two assumptions, as follows. First, we assume that ships sailing in ice area are not affected by wind, wave and current, the total resistance R is determined by calm water resistance $\mathrm{R_{SW}}$ and ice resistance $\mathrm{R_{ice}}$

$$\mathrm{R_T} = \mathrm{R_{SW}} + \mathrm{R_{ice}} \quad (5)$$

where $\mathrm{R_{SW}}$ can be obtained from open water model experiments and its calculation formula is as follows

$$\mathrm{R_{SW}} = 0.5\rho_w S\overline{C_{SW}} \cdot V^2 = \mathrm{a}V^2 \quad (6)$$

where ρ_w and S are water density and wetted surface area of the ship, respectively. The calm water resistance coefficient C_{SW} is always assumed to be constant, and V is the ship speed. We express $\mathrm{R_{SW}}$ as $\mathrm{a}V^2$, and $\mathrm{a} = 0.5\rho_w S\overline{C_{SW}}$.

The ice resistance force, $\mathrm{R_{ice}}$, is defined as

$$\mathrm{R_{ice}} = 0.5C_P\rho_i B h_i C^n \cdot V^2 \quad (7)$$

where C_P is the ice force coefficient, ρ_i, B, h_i and C are the ice density, ship beam, ice thickness and ice concentration, respectively. The value of the power of ice concentration, n=2, is consistent with the analysis of Colbourne[40]. Guo et al.[41] uses non-dimensional analysis to get the relationship between the ice resistance coefficient C_P and ice Froude number Fr_P based on the experiment of Institute of Ocean Technology as follows

$$C_P = 4.4Fr_P^{-0.8267} \tag{8}$$

where Fr_P is related to ice thickness and ice concentration, and g is the acceleration of gravity.

$$Fr_P = \frac{V}{\sqrt{gh_iC}} \tag{9}$$

Second, we assume that the effective power P_e in calm water is the same as ice conditions, which satisfies

$$P_e = \mathrm{R_{SW}}(V_{SW})V_{SW} = \mathrm{R_T}(V_r)V_r = [\mathrm{R_{SW}}(V_r) + \mathrm{R_{ice}}(V_r)]V_r \tag{10}$$

where V_{SW} and V_r are calm water speed and actual speed.

To simplify the equation above, we further assume that $\mathrm{R_{ice}}(V_r) = \mathrm{R_{ice}}(V_{SW})$, which is more reasonable than just assuming $\mathrm{R_{ice}}(V_r)V_r = \mathrm{R_{ice}}(V_{SW})V_{SW}$ according to Sen[42]. Then the real reduced speed is given as

$$\mathrm{a}V_{SW}^2 = \mathrm{a}V_r^2 + \mathrm{R_{ice}}(V_{SW}) \tag{11}$$

where

$$V_r = (V_{SW}^2 - \frac{R_{ice}(V_{SW})}{a})^{0.5} \tag{12}$$

After obtaining the V_r based on sea ice condition, we introduce a deceleration coefficient ζ to demonstrate how sea fog can influence the speed of ship (Table S5). The higher SFF on a given grid, the larger deceleration coefficient will be. The V_r on the grid will be multiplied by (1- ζ). Then A* algorithm is implemented to calculate the route between two points that accumulates the lowest total time. A* is a modification of the least cost path algorithm, using a heuristic to determine which vertices to search.

Finally, the Route-F is derived as the optimal Arctic shipping route with minimum sailing time.

Data availability

International Comprehensive Ocean-Atmosphere Data Set (ICOADS) Observations are available from https://rda.ucar.edu/datasets/ds548.0/. 6-hourly ERA-Interim data are available from https://apps.ecmwf.int/datasets/. CMIP5 data used in the paper are available from https://esgf-node.llnl.gov/search/cmip5/.

Code availability

The Polar WRF package is available from http://polarmet.osu.edu/PWRF/. Codes used to design shipping routes in the study are available from the corresponding author on reasonable request.

References

27. Bromwich, D. H., Hines, K. M. & Bai, L. Development and testing of Polar Weather Research and Forecasting model: 2. Arctic Ocean. *J. Geophys. Res.* **114**, D08122 (2009).
28. Hong, S.-Y. & Lim, J.-O. The WRF single-moment 6-class microphysics scheme (WSM6). *J. Korean Meteor. Soc.* **42**, 129–151 (2006).
29. Clough, S. A. *et al.* Atmospheric radiative transfer modeling: A summary of the AER codes. *J. Quant. Spectrosc. Radiat. Transf.* **91**, 233–244 (2005).
30. Nakanishi, M. & Niino, H. An improved Mellor-Yamada Level-3 model: Its numerical stability and application to a regional prediction of advection fog. *Boundary-Layer Meteorol.* **119**, 397–407 (2006).
31. Grell, G. A. & Freitas, S. R. A scale and aerosol aware stochastic convective parameterization for weather and air quality modeling. *Atmos. Chem. Phys.* **14**, 5233–5250 (2014).
32. Hines, K. M. & Bromwich, D. H. Simulation of late summer arctic clouds during ASCOS with polar WRF. *Mon. Weather Rev.* **145**, 521–541 (2017).
33. Stoelinga, M. T. & Warner, T. T. Nonhydrostatic, mesobeta-scale model simulations of cloud ceiling and visibility for an East Coast winter precipitation

event. *J. Appl. Meteorol.* **38**, 385–404 (1999).

34. Doran, J. A., Roohr, P. J. & Beberwyk, D. J. The MM5 at the Air Force Weather Agency—New products to support military operations. in *The 8th Conference on Aviation, Range, and Aerospace Meteorology, NOAA/NWS, Dallas, Texas.* 1999 (1999).
35. Gultepe, I., Müller, M. D. & Boybeyi, Z. A new visibility parameterization for warm-fog applications in numerical weather prediction models. *J. Appl. Meteorol. Climatol.* **45**, 1469–1480 (2006).
36. Gultepe, I. *et al.* The Fog Remote Sensing and Modeling Field Project. *Bull. Am. Meteorol. Soc.* **90**, 341–360 (2009).
37. Ngai, S. T., Tangang, F. & Juneng, L. Bias correction of global and regional simulated daily precipitation and surface mean temperature over Southeast Asia using quantile mapping method. *Glob. Planet. Change* **149**, 79–90 (2017).
38. Government of Canada. *Arctic Ice Regime Shipping System (AIRSS) standard*. *Transport Canada* (1998).
39. Colbourne, D. B. Scaling pack ice and iceberg loads on moored ship shapes. *Ocean. Eng. Int.* **4**, 39–45 (2000).
40. Woolgar, R. C. & Bruce Colbourne, D. Effects of hull-ice friction coefficient on predictions of pack ice forces for moored offshore vessels. *Ocean Eng.* **37**, 296–303 (2010).
41. Guo, C. yu, Xie, C., Zhang, J. zhao, Wang, S. & Zhao, D. gang. Experimental Investigation of the Resistance Performance and Heave and Pitch Motions of Ice-Going Container Ship Under Pack Ice Conditions. *China Ocean Eng.* **32**, 169–178 (2018).
42. Sen, D. & Padhy, C. P. An approach for development of a ship routing algorithm for application in the North Indian Ocean region. *Appl. Ocean Res.* **50**, 173–191 (2015).

Acknowledgements

X.C. was supported by the National Key R&D Program of China under Grant 2019YFA0607000, and Belmont Forum and the Natural Science Foundation of China under Grant 41825012 and 41561144001. J. Z. was supported by the Natural Science Foundation of China under Grant 41941012 and 41976022.

Author contributions

X.C. led this research. S. S. undertook the model simulation and analysis, and led the draft of this manuscript. Y. C. develop the new algorithm to design the Arctic shipping routes. C. C. developed the model settings. K. L., K.-K.T., Q. S., Y. L., X. W., L. Y. and J. Z. provided constructive suggestions for improving the research and writing. Authors contributed substantially to the drafting and revision of this manuscript.

Competing interests

The authors declare no competing interests.

Supplementary Files

This is a list of supplementary files associated with this preprint. Click to download.

- Supplementaryinformation20220130.pdf